Research Article

A study of ^{12}c +^{12}c nuclear reaction using a new M3Y-type effective interaction

Isaiah Ochala[1]* Daniel Terver[2] and Joseph O Fiase[2]

[1]Department of Physics, Kogi State University, Nigeria

[2]Department of Physics, Benue State University, Makurdi, Nigeria

Abstract

This paper is a study of nuclear reactions involving ^{12}C + ^{12}C nuclei carried out with a heavy-ion nucleus-nucleus optical potential derived from a new M3Y-type effective interaction, called B3Y-Fetal, within the framework of optical model at the incident energies of 112, 126.7, 240, 300, 1016 MeV. Folding analyses of the differential cross sections associated with the elastic scattering of the nuclear system, determined at these incident energies with four B3Y-Fetal-based folded potentials constructed from double folding model, have shown the DDB3Y1- and BDB3Y1-Fetal potentials to be the best in excellent agreement with previous work done with the M3Y-Reid. The agreement of the B3Y-Fetal with the famous M3Y-Reid effective interaction, which is also used for folding analysis in this work, is further buttressed and well-established by the findings of this study Herein, the values of the renormalization factor, NR ranging from 1.1117 to 0.8121, obtained with the B3Y-Fetal have been found to be slightly higher, with lower reaction cross sections, a_R = 1418 - 1047 millibarns, than N_R = 0.9971 - 0.8108 obtained with the M3Y-Reid effective interaction whose accompanying reaction cross sections, being higher, range from 1431 to 1050 millibarns. This depicts the B3Y-Fetal as having a better performance. Additionally, results of folding analyses have shown the best-fit folded potentials, DDB3Y1- and BDB3Y1-Fetal potentials to be in agreement at all incident energies, implying that the cold nuclear matter has an underlying soft equation of state.

Introduction

Nuclear reaction takes place when a nucleon or nucleus collides with another nucleon or nucleus. The characteristics of the nuclear reactions induced by nucleons or nuclei are summarized in distributions of reaction products called cross-sections [1]. Nuclear reactions are studied in nuclear scattering experiments, among which elastic scattering is believed to be the simplest [2-4] because it involves very little rearrangement of matter and energy [5]. This process has been studied in a large number of theoretical and experimental investigations for more than forty years, so a huge body of elastic cross-section data is currently available [5].

Experimentally, the establishment of many radioactive beam facilities around the world such as the Cooling Storage Ring (CSR) facility HIRFL in China, the Radioactive Ion Beam (RIB) Factory at RIKEN in Japan, the FAIR/GSI in Germany, SPIRAL2/GANIL in France and the facility for Rare Isotope Beams (FRIB) in USA has made it possible to study heavy-ion reactions fairly explicitly in terrestrial laboratories. Knowledge gained from these reactions is important for understanding not only the structure of radioactive nuclei, the equation of state (EOS) of symmetric and asymmetric of nuclear matter, the reaction dynamics induced by rare isotopes and the liquid-gas phase transition in asymmetric nuclear matter, but also many critical issues in Astrophysics.

To study the average features of the collision between two nuclei such as elastic scattering and the gross absorption of the incident flux into non-elastic channels, the optical model (OM) is one of the most widely and successfully used nuclear models [6,7]. The earliest optical potential used in many analyses was a phenomenological local potential, having a Woods-Saxon functional form, whose parameters were varied to yield a good fit to experimental data [8]. The nuclear part of the potential consists of a real and a complex (imaginary) part which allows for volume or surface absorption. This form of optical potential has been used in OM analyses of elastic data [6,9] with good success, but is now used with decreasing popularity, most especially in refractive heavy-ion scattering where there is increasing understanding of the real part of the potential from first principles. The newer approach in OM

analyses is an optical potential derived in the framework of macroscopic approximation using nuclear matter properties, nuclear surface, density distributions of nuclei and a simple effective nucleon-nucleon (NN) interaction. A very convenient way of incorporating gross nuclear matter properties in OM analyses is through the use of folding models [2] believed to be one of the most successful models used for years to calculate the nucleon-nucleus and nucleus-nucleus optical potentials. In this approach, the optical potential is generated by folding an effective nucleon-nucleon interaction over the ground-state density distributions of the two nuclei [10-12]. The effective nucleon-nucleon (NN) interaction is usually based on a realistic NN force because the goal in OM analyses is to obtain a unified description of the nucleon-nucleon, nucleon-nucleus and nucleus-nucleus scattering [5].

Theoretically, the M3Y-type effective interaction, along with the nuclear densities of the target and projectile nuclei, has consistently been a popular choice in the folding model [13,14] to calculate the nucleon-nucleus and nucleus-nucleus potentials. For this reason, we principally use our new M3Y-type effective interaction, the B3Y-Fetal, in its energy- and density-dependent form alongside appropriately chosen nuclear projectile and target densities in a double folding model to construct a nucleus- nucleus heavy-ion (HI) optical potential meant for the study of the elastic scattering of ^{12}C +^{12}C nuclei at various collision energies with the intent to evaluate the differential cross sections of the different nuclear reactions in this study. In doing this, the density dependences to use are the DDM3Y1, BDM3Y1, BDM3Y2 and BDM3Y3. When the B3Y-Fetal effective interaction is used in these density-dependent versions, they will be called the DDB3Y1 -Fetal, BDB3Y1-Fetal, BDB3Y2-Fetal and BDB3Y3-Fetal interactions respectively. Different density-dependent versions of the M3Y-Reid and M3Y-Paris interactions, which generated different values of incompressibility, K of the cold nuclear matter within the Hartree-Fock (HF) formalism, have been used either in the single folding [15] or double folding model [9,12,16] previously For comparative purposes, the B3Y-Fetal is to be used in the named density-dependent versions along with the M3Y-Reid interaction. Like the the M3Y-Reid and M3Y-Paris interactions, the B3Y- Fetal has been used in symmetric [17,18] and asymmetric [19,20] nuclear matter calculations with agreeably impressive and convincing results; and this study is a further test of the viability of the new M3Y-type effective interaction. In this light, folding analyses to be carried out in this study are a computational necessity for a complete description of the form and character of the B3Y-Fetal interaction.

The ^{12}C +^{12}C system chosen for the study of elastic scattering in this work is one of the most widely studied combinations of light heavy ions, so there is a relative abundance of experimental data at low and intermediate energies for the folding analyses of nuclear reactions involving them. In addition, this nuclear system is known to exhibit weak absorption in elastic scattering so that refractive scattering takes place in it. The refractive scattering in this work provides a very important information on the EOS of the cold nuclear matter and helps to determine the real component of HI optical potential down to small inter-nuclear distances, giving the possibility of testing different theoretical models for heavy- ion optical potential. Therefore, this study affords us the opportunity to test and establish the viability of the theoretical model used for developing the B3Y-Fetal by helping us to determine the goodness of the HI optical potential based on the new B3Y-Fetal. In pursuit of this, we use the famous M3Y-Reid along with the B3Y-Fetal effective interaction as a measuring yardstick for determining the performance of the latter. In terms of organization, the rest of the paper is structured such that Section 2 describes the salient features of the HI optical potential tersely while Section 3 presents and discusses the results of the study.

The heavy ion optical potential

The heavy ion optical potential for the study of ^{12}C +^{12}C nuclear reaction isgenerated using a double folding model in which the B3Y-Fetal effective interaction is folded with the nuclear densities of the identical nuclei in this work.

The radial form of the isoscalar part of the B3Y-Fetal NN interaction is given in terms of three Yuka was as [21]:

$$v^D(r) = \frac{10472.13e^{-4r}}{4r} - \frac{2203.11e^{-2.5r}}{2.5r}$$

$$v^{EX}(r) = \frac{499.63e^{-4r}}{4r} - \frac{1347.77e^{-2.5r}}{2.5r} - \frac{7.8474e^{-07072r}}{0.7072r} \qquad (1)$$

Similarly, the functional form of the M3Y-Reid NN interaction is expressed in terms of three Yuka was as [13,22,23]:

$$v^D(r) = \frac{7999.00e^{-4r}}{4r} - \frac{2134.25e^{-2.5r}}{2.5r}$$

$$v^{EX}(r) = \frac{4631.375e^{-4r}}{4r} - \frac{1787.125e^{-2.5r}}{2.5r} - \frac{7.8474e^{-07072r}}{0.7072r} \qquad (2)$$

To be able to reproduce the saturation properties of nuclear matter correctly, a density-dependence is usually introduced into the M3Y-type effective interaction. The density-dependent effective interaction has the form:

$$v^{D(EX)}(\rho, r) = g(E)F(\rho)v^{D(EX)}(r), \qquad (3)$$

where F(ρ) is the density dependent factor whose explicit forms are

$$F(\rho) = C_o(1 + \alpha e^{-\beta\rho}) \qquad (4)$$

and

$$F(\rho) = C_o(1 + \alpha\rho^\beta) \qquad (5)$$

Representing the DDM3Yn $(n = 1)$ and BDM3Yn $(n = 0, 1, 2, 3)$ interactions respectively. With these density dependences introduced into the B3Y-Fetal effective interaction, it was applied in our earlier paper to nuclear matter calculations, reproducing the saturation properties of the cold nuclear matter at density $p_0 = 0.17/m^{-3}$ and binding energy, E/A =16 MeV in excellent agreement with M3Y-Reid and M3Y-Paris effective interactions.

For the study of nuclear reactions, an energy dependence is added to the density-dependent interaction of Equation (3) so that the nucleon optical potential has the functional form:

$$v^{D(EX)} (E,\rho,\mathbf{r}) = g(E)F(\rho)v^{D(EX)} (\mathbf{r}), \qquad (6)$$

where $g(E) \sim 1-0.002$ E for the M3Y-Reid [12,23,24] as well as B3Y-Fetal [25]; and E is the incident nucleon energy. This energy- and density-dependent interaction is known to work well in folding model analyses of the elastic, refractive o-nucleus [26] and nucleus-nucleus [13,16,27] scattering; and this is the form in which the B3Y-Fetal is used alongside the M3Y-Reid in the folding model in this work.

The folding procedure generates the real part of the nucleus-nucleus optical potential, which is evaluated as an antisymmetrized Hartree-Fock-type potential of the form [2,11,12,27]:

$$V_{ij} = \sum_{i\in A_1, j\in A_2} \left[ij|v^D|ij + ij|v^{EX}|ji \right] \qquad (7)$$

where $|i\rangle$ and $|j\rangle$ are single-particle wave functions of nucleons i and j in the two colliding nuclei A_1 and A_1 respectively; and v^D and v^{EX} are the direct and exchange potential components of the effective interaction with which the densities of the projectile and target nuclei are folded to have a direct and an exchange component of the optical potential as [12]:

$$V_D (E,\mathbf{R}) = \int \rho_1(\mathbf{r_1})\rho_2(\mathbf{r_2})V^D (\rho,E,s)d\mathbf{r_1}\, d\mathbf{r_2} \qquad (8)$$

With $\mathbf{s} = \mathbf{r_1} - \mathbf{r_2} + \mathbf{R}$

$$V_{EX} (E,\mathbf{R}) = \int\rho_1(\mathbf{r_1}, \mathbf{r_1}+\mathbf{s})\rho_2(\mathbf{r_2}, \mathbf{r_2} - \mathbf{s})V^{EX} \times \exp\frac{[i\mathbf{K}(\mathbf{R})\mathbf{s}]}{M}d\mathbf{r_1}d\mathbf{r_2} \qquad (9)$$

where ρ_1 and ρ_2 are the densities of the interacting nuclei, $\mathbf{s} = \mathbf{r_1} - \mathbf{r_2} + \mathbf{R}$ is a vector corresponding to the distance between two specified interacting points of the projectile and target whose radius vectors are $\mathbf{r_1}$ and $\mathbf{r_2}$ respectively; and R is the vector joining the centres of mass of the two nuclei. While the direct component is local in coordinate space, the exchange component is non-local. The exchange potential is evaluated in this work using an exact, finite- range method which involves treating the relative motion locally as a plane wave so that the local momentum of relative motion is:

$$K^2(\mathbf{R}) = \frac{2mM}{\hbar^2}[E_{c.m} - V(E,\mathbf{R}) - V_C(\mathbf{R})] \qquad (10)$$

where $M = \frac{A_1 A_2}{(A_1 + A_2)}$ is the reduced mass, $E_{c.m}$ the centre-of-mass (c.m)energy, E the incident laboratory energy per nucleon and m the bare nucleon mass $V(E,\mathbf{R}) = V_D (E,\mathbf{R}) + V_{EX} (E,\mathbf{R})$ is the total nuclear potential and $V_C(\mathbf{R})$ is the Coulomb potential.

Through a series of steps involving mixed-density expansion and extended Thomas-Fermi approximation, a local, energy-dependent exchange term is obtained in the form [12,23,24]:

$$V_{EX} (E,\mathbf{R}) = 4\pi g(E)\int_0^\infty v^{EX} (s)s^2 ds j_0\left(\frac{k(\mathbf{R})s}{M}\right) \qquad (11)$$
$$\times\int f_1(\mathbf{r},s) f_2(\mathbf{r}-\mathbf{R},s)\times F\left[\rho_1(\mathbf{r}) + \rho_2(\mathbf{r}-\mathbf{R})\right]dr,$$

Where $f_{1(2)}(\mathbf{r},s) = \rho_{1(2)}(\mathbf{r})J_1 (k_{F1(2)}(\mathbf{r})s)$ and $j_0(x) = \sin x/x$

$$V_{EX} (E,\mathbf{R}) = 4\pi g(E)\int_0^\infty G(R,s) j_0(k(\mathbf{R})s / M)v^{EX}(s)s^2 ds \qquad (12)$$

where

$$G(\mathbf{R},s) = \frac{C}{2\pi}\int_0^\infty [h_1(t,s)h_2(t,s)\alpha\overline{G(t,s)}]j_0(t\mathbf{R})t^2 dt \qquad (13)$$

and $h_{1(2)} = 4\pi\int_0^\infty f_{1(2)}(r,s) j_0(tr)r^2 dr.$

The explicit form of the function $\overline{G(t,s)}$ is determined by the explicit form of the density-dependent function $F(\rho)$ used. Thus,

$$\overline{G(t,s)} = \begin{cases} y_1(t,s) y_2(t,s) & DDM3Y1 - type\ Interaction: \\ -\sum_{n=0}^{\beta}\binom{\beta}{n} z_1^{(\beta-n+1)}(l,s) z_2^{(n+1)}(l,s) & BDM3Y - type\ Interaction: \end{cases} \qquad (14)$$

Here,

$$y_{1(2)} = 4\pi\int_0^\infty f_{1(2)}(r,s)\exp\left[-\beta\rho_{1(2)}(r)\right]\times j_0(tr)r^2 dr$$

and

$$z_{1(2)}^{(m)}(t,s) = 4\pi\int_0^\infty f_{1(2)}\rho_{1(2)}^m(r)r^2 dr$$

The exchange potential is evaluated by exact iterative method herein. Since it is known from calculation that the energy dependence of the total folded potential, V(E,**R**) on the exchange term is much stronger than its dependence on the intrinsic energy dependence, g(E) [2,11,23], accurate evaluation of the knock-on exchange effects is ensured in this work. Here, an insight into the energy dependence of the optical potential is provided by the volume integral of the folded potential per interacting nucleon pair expressed as [11,23]:

$$J_R(E) = \frac{4\pi N_R}{A_1 A_2}\int_0^\infty \left[V_D(E,r) + V_{EX}(E,r)\right]r^2 dr \qquad (15)$$

This parameter is a sensitive measure of the potential strength.

In the final analysis, the heavy ion nucleus-nucleus optical potential for the study of ^{12}C +^{12}C nuclear reaction at the incident energies of 112, 126.7, 240, 300 and 1016 MeV in this paper is composed of the double folding model as the real part and a phenomenological Woods-Saxon shape as the imaginary part. The total real folded potential, resulting from the double folding model is real because the B3Y-Fetal as well as the M3Y-Reid is real. This real folded potential, V(E,**R**) consisting of direct, V_D(E,**R**) and exchange, V_{EX}(E,**R**) parts expressed as shown in equations (8) and (9), enters the optical model analyses, accounting for elastic scattering. The imaginary part (Woods-Saxon (WS) shape), whose parameters are adjusted to give the best fit to the scattering data, represents non-elastic processes believed to cause the absorption of incident particles in nuclear reactions [28]. Thus, the HI optical potential in our optical model calculations is [12]:

$$U(E,R) = N_R \left[V_D(E,\ R) + V_{EX}(E,R) \right] - iW_V \left[1 + exp\left(\left(\frac{R - R_V}{a_v} \right) \right) \right] \quad (16)$$

where W_V, a_v and $\mathbf{R}_V$ are the strength, diffuseness and radius of the volumeterms of the Woods-Saxon function respectively [29]. We adjust these parametersalongside the normalization factor, N_R to obtain best fits to the elastic scattering angular distributions. All the nuclear densities in the folding model are taken as a Fermi distribution with parameters that can reproduce the shell-model densities for the nuclei under consideration. All computational analyses of the optical model are to be carried out using the ECIS-97 code.

Results and discussion

The folding analyses of the elastic scattering of ^{12}C +^{12}C nuclear system at different incident energies within the framework of optical model were successfully performed with the B3Y-Fetal and M3Y-Reid interactions in their DDM3Y1, BDM3Y1, BDM3Y2 and BDM3Y3 density-dependent versions in this paper. Results of the folding analyses, presented in tables 1.0 a - 1.0 f and Figures 1.0 - 7.0, show the B3Y-Fetal effective interaction to be in excellent agreement with the M3Y-Reid interaction. It is worthy of mention that this most widely studied HI system has been found to be characterized by very weak absorption in the low-energy data in agreement with [12], making the occurrence of nuclear rainbow possible in the angular distribution. In discussing the results obtained with the four types of the real folded potential in table 1.0, the performance of the B3Y-Fetal effective interaction at the various incident energies is first generally discussed and then compared with the M3Y-Reid whenever the need arises.

At the incident energy of 112 MeV, Figure 1.0 presents the DDB3Y1-Fetal, BDB3Y1-Fetal and BDB3Y2-Fetal in the upper region as the folded potentials with reasonably good fits, while the DDM3Y1-Reid, BDM3Y1-Reid and BDM3Y2-Reid are also shown in the lower region as the potentials with acceptable fits. These best-fit folded potentials have N_R values (Table 1.0a) that are very close to 1, indicating that the effect of dynamical polarization is very weak. The BDB3Y3- Fetal as well as the BDM3Y3-Reid potential has a very different shape as well as slope, making it unable to reproduce the large-

(a) ^{12}C+^{12}C, E_{Lab} = 112MeV

Potential	N_R	$- J_R$ (MeV fm^3)	$\langle r_R^2 \rangle^{\frac{1}{2}}$ (fm)	W_V (MeV)	R_V (fm)	a_V (fm)	σ_R (mb)	χ^2
DDM3Y1-REID	0.9085 (0.9954) 0.9296	336.1 (336.6) 346.3	3.8400 (3.7950) 3.8041	19.229 (18.259) 18.720	5.1753 (5.1753) 5.1753	0.6679 (0.6679) 0.6679	1397 (1393) 1390	8.84 (15.8) 11.72
BDM3Y1-REID	0.9348 (1.0298) 0.9463	345.9 (339.6) 345.0	3.8454 (3.8029) 3.8086	18.3191 (18.123) 17.936	5.2134 (5.2134) 5.2134	0.6563 (0.6563) 0.6563	1398 (1391) 1388	7.7 (15.2) 11.5
BDM3Y2-REID BDB3Y2-FETAL	0.9971 (1.1198) 1.0126	349.9 (348.5) 351.5	3.8656 (3.8291) 3.8261	17.6050 (17.605) 17.605	5.3385 (5.3385) 5.3385	0.6171 (0.6171) 0.6171	1386 (1383) 1381	7.5 (13.5) 11.1
BDM3Y3-REID BDB3Y3-FETAL	0.8706 (0.9832) 1.1117	304.9 (279.5) 313.7	3.8969 (3.9105) 4.1386	15.305 (15.305) 15.305	5.4541 (5.4541) 5.4541	0.5949 (0.5949) 0.5949	1358 (1354) 1373	20.6 (32.8) 6.7

(b) ^{12}C+^{12}C, E_{Lab} = 126.7MeV

Potential	N_R	$- J_R$ (MeV fm^3)	$\langle r_R^2 \rangle^{\frac{1}{2}}$ (fm)	W_V (MeV)	R_V (fm)	a_V (fm)	σ_R (mb)	χ^2
DDM3Y1-REID	0.8885 (0.9873) 0.9422	332.7 (330.9) 346.8	3.8405 (3.7967) 3.8046	17.949 (17.949) 17.949	5.3708 (5.3708) 5.3708	0.5810 (0.5810) 0.5810	1355 (1350) 1354	7.7 (10.0) 9.00
BDM3Y1-REID BDB3Y1-FETAL	0.9110 (1.0188) 0.9721	333.2 (332.9) 350.1	3.8460 (3.8047) 3.8091	17.960 (17.960) 17.960	5.3836 (5.3836) 5.3836	.5790 (0.5790) .5790	1357 (1353) 1356	8.1 (9.6) 9.0
BDM3Y2-REID BDB3Y2-FETAL	0.9895 (1.0981) 1.0487	343.2 (338.6) 359.6	3.8663 (3.8309) 3.8268	18.271 (18.271) 18.271	5.4031 (5.4031) 5.4031	0.5762 (0.5776) 0.5762	1367 (1363) 1365	8.5 (9.3) 9.2
BDM3Y3-REID BDB3Y3-FETAL	0.9734 (0.9734) 1.0760	337.1 (274.1) 299.4	3.8975 (3.9036) 4.1428	17.443 (17.443) 17.443	5.3844 (5.3844) 5.3844	0.5722 (0.5722) 0.5722	1346 (1332) 1350	9.7 (18.1) 8.4

Table 1: Optical Parameters Used in the Folding Analyses of the Elastic ^{12}C +^{12}C Scattering Data at E_{Lab} = 112 — 1449 MeV. The results obtained in Ref. [12] with M3Y-Reid interaction are in brackets.

Potential	N_R	$-J_R$ (MeV fm³)	$\langle r_R^2\rangle^{1/2}$ (fm)	W_V (MeV)	R_V (fm)	a_V (fm)	σ_R (mb)	χ^2
DDM3Y1 -REID	0.8121	278.7	3.8457	28.849	5.894	0.6397	1392	34.0
	(0.9253)	(288.8)	(3.8110)	(28.649)	(5.0754)	(0.6394)	(1383)	(42.2)
BDM3Y1 -REID	0.8121	272.4	3.8098	28.849	5.0894	0.6397	1388	18.1
BDB3Y1 -FETAL	0.8269	277.0	3.8518	28.970	5.918	0.6370	1390	31.8
	(0.9569)	(291.1)	(3.8192)	(28.870)	(5.0918)	(0.6370)	(1388)	(43.1)
BDM3Y2 -REID	0.8269	271.3	3.8147	28.970	5.0918	0.6370	1387	19.3
BDB3Y2 -FETAL	0.8545	271.1	3.8733	29.929	5.1180	0.6317	1401	27.6
	(1.0345)	(296.7)	(3.8460)	(29.929)	(5.1180)	(0.6317)	(1403)	(46.2)
BDM3Y3 -REID	0.8545	266.6	3.8333	29.929	5.1180	0.6317	1398	21.5
BDB3Y3 -FETAL	0.8497	270.2	3.9033	29.801	5.1378	0.6247	1398	36.7
	(0.9477)	(247.9)	(3.9196)	(27.401)	(5.1378)	(0.6247)	(1374)	(46.1)
	0.8497	211.7	4.1782	29.801	5.1378	0.6247	1395	23.8

(c) ^{12}C+^{12}C, E_{Lab} = 240MeV

Potential	N_R	$-J_R$ (MeV fm³)	$\langle r_R^2\rangle^{1/2}$ (fm)	W_V (MeV)	R_V (fm)	a_V (fm)	σ_R (mb)	χ^2
DDM3Y1 -REID	0.8108	265.8	3.8494	28.835	5.461	0.6916	1419	12.4
	(0.9307)	(279.7)	(3.8190)	(28.349)	(5.0461)	(0.6916)	(1413)	(23.2)
	0.8439	269.4	3.8135	28.828	5.0461	0.6916	1418	10.6
BDM3Y1 -REID	0.8270	264.6	3.8557	28.1786	5.917	0.6827	1419	13.2
	(0.9545)	(279.6)	(3.8274)	(27.747)	(5.0917)	(0.6827)	(1417)	(25.4)
	0.8585	268.0	3.8186	28.1313	5.0917	0.6827	1417	11.2
BDM3Y2 -REID	0.8636	261.5	3.8778	27.4641	5.1503	0.6726	1421	15.5
	(1.0120)	(279.4)	(3.8546)	(27.256)	(5.1503)	(0.6726)	(1419)	(30.7)
BDB3Y2 -FETAL	0.8811	261.5	3.8378	27.287	5.1503	0.6726	1418	12.8
BDM3Y3 -REID	0.8505	258.7	3.9070	26.0360	5.2630	0.6572	1431	16.8
	(1.0577)	(266.1)	(3.9285)	(25.412)	(5.2630)	(0.6572)	(1424)	(39.6)
BDB3Y3 -FETAL	0.8555	200.9	4.1990	23.963	5.2630	0.6572	1404	17.22

(d) ^{12}C+^{12}C, E_{Lab} = 300MeV

Table 1: c,d

Potential	N_R	$-J_R$ (MeV fm³)	$\langle r_R^2\rangle^{1/2}$ (fm)	W_V (MeV)	R_V (fm)	a_V (fm)	σ_R (mb)	χ^2
DDM3Y1 -REID	0.9212	180.0	3.9305	17.883	5.714	0.8371	1205	9.0
	(0.9212)	(181.4)	(3.9280)	(17.683)	(5.0714)	(0.8371)	(1199)	(18.1)
	0.9212	162.7	3.9101	17.883	5.0714	0.8371	1198	9.5
BDM3Y1 -REID	0.9517	181.1	3.9392	17.1660	5.1652	0.8210	1209	9.7
	(0.9517)	(182.4)	(3.9376)	(16.966)	(5.1652)	(0.8210)	(1203)	(21.9)
	0.9517	164.0	3.9172	16.966	5.1652	0.8210	1202	8.9
BDM3Y2 -REID	1.300	184.3	3.9668	16.3430	5.2726	0.8294	1238	13.6
	(1.0300)	(185.3)	(3.9675)	(16.143)	(5.2726)	(0.8294)	(1231)	(38.6)
BDB3Y2 -FETAL	1.0300	167.7	3.9408	16.143	5.2726	.0.8294	1230	9.3
BDM3Y3 -REID	0.9006	167.0	3.9764	17.186	5.2171	0.8253	1234	14.6
	(1.1006)	(179.5)	(4.0451)	(17.186)	(5.2171)	(0.8253)	(1236)	(104.7)
BDB3Y3 -FETAL	0.9006	101.2	4.5815	17.186	5.2171	0.8253	1231	41.8

(e) ^{12}C+^{12}C, E_{Lab} = 1016MeV, Imag. WS(I)Pot.

Potential	N_R	$-J_R$ (MeV fm³)	$\langle r_R^2\rangle^{1/2}$ (fm)	W_V (MeV)	R_V (fm)	a_V (fm)	σ_R (mb)	χ^2
DDM3Y1 -REID	0.9572	189.0	3.9305	49.483	3.6925	0.8315	1062	10.1
	(0.9572)	(188.5)	(3.9280)	(49.283)	(3.6925)	(0.8315)	(1060)	(8.8)
	0.9572	169.0	3.9101	49.483	3.6925	0.8315	1059	6.7
BDM3Y1 -REID	0.9784	186.1	3.9392	50.0090	3.6793	0.8314	1061	10.4
	(0.9784)	(187.5)	(3.9376)	(49.809)	(3.6793)	(0.8314)	(1059)	(8.7)
	0.9784	168.6	3.9172	49.809	3.6793	0.8314	1057	6.4
BDM3Y2 -REID	1.251	183.5	3.9668	50.636	3.6569	0.8323	1058	11.3
	(1.0251)	(184.5)	(3.9675)	(50.436)	(3.6569)	(0.8323)	(1056)	(8.6)
BDB3Y2 -FETAL	1.0251	167.0	3.9408	50.436	3.6569	0.8323	1054	5.5
BDM3Y3 -REID	0.8854	164.2	3.9764	50.90	3.6341	0.8376	1050	13.0
	(1.0854)	(177.0)	(4.0451)	(50.0090)	(3.6341)	(0.8376)	(1051)	(9.8)
BDB3Y3 -FETAL	0.8854	99.5	4.5815	50.0090	3.6341	0.8376	1047	19.8

(f) ^{12}C+^{12}C, E_{Lab} = 1016MeV, Imag. WS(II)Pot.

Table 1: e,f

Potential	N_R	$-J_R$ (MeV fm^3)	$\langle r^2_R \rangle^{1/2}$ (fm)	W_V (MeV)	R_V (fm)	a_V (fm)	σ_R (mb)	χ^2
DDM3Y1 -REID DDB3Y1 -FETAL	0.9168 (0.9168) 0.9168	134.3 (142.9) 111.9	4.0025 (4.0055) 4.0178	12.255 (12.255) 12.255	5.4093 (5.4093) 5.4093	1.54 (1.0054) 1.0054	1191 (1191) 1189	3.2 (26.1) in
BDM3Y1 -REID BDB3Y1 -FETAL	0.9376 (0.9376) 0.9376	133.6 (142.1) 111.6	4.0120 (4.0156) 4.0257	11.9010 (11.701) 11.701	5.4810 (5.4810) 5.4810	1.301 (1.0301) 1.0301	1221 (1210) 1209	3.3 (27.1) 7.9
BDM3Y2 -REID BDB3Y2 -FETAL	0.9937 (0.9937) 0.9937	132.9 (141.2) 111.5	4.0417 (4.0464) 4.0506	10.563 (10.363) 10.363	5.7173 (5.7173) 5.7173	1.531 (1.0531) 1.0531	1258 (1245) 1244	4.2 (30.4) 8.3
BDM3Y3 -REID BDB3Y3 -FETAL	0.8978 (1.0978) 0.8978	127.2 (141.1) 61.1	4.0313 (4.1248) 4.9952	10.121 (10.121) 10.121	6.2735 (6.2735) 6.2735	1.483 (1.0483) 1.0483	1462 (1259) 1460	4.0 (40.7) 22.3

(g) ^{12}C+^{12}C, E_{Lab} = 1449MeV, Imag. WS(I)Pot.

Potential	N_R	$-J_R$ (MeV fm^3)	$\langle r^2_R \rangle^{1/2}$ (fm)	W_V (MeV)	R_V (fm)	a_V (fm)	σ_R (mb)	χ^2
DDM3Y1 -REID	0.9551 (0.9551) 0.9551	139.9 (148.9) 116.6	4.0025 (4.0055) 4.0178	45.052 (44.852) 44.852	3.7350 (3.7350) 3.7350	.07809 (0.7809) 0.7809	929 (927) 925	2.2 (20.4) 3.8
BDM3Y1 -REID BDB3Y1 -FETAL	0.9732 (0.9732) 0.9732	138.6 (147.5) 115.8	4.0120 (4.0156) 4.0257	44.709 (44.509) 44.509	3.7333 (3.7333) 3.7333	0.7783 (0.7783) 0.7783	923 (921) 919	1.3 (19.6) 3.7
BDM3Y2 -REID BDB3Y2 -FETAL	1.163 (1.0163) 1.0163	135.9 (144.4) 114.1	4.0417 (4.0464) 4.0506	43.253 (43.053) 43.053	3.7411 (3.7411) 3.7411	0.7729 (0.7729) 0.7729	909 (908) 906	1.2 (17.6) 3.5
BDM3Y3 -REID BDB3Y3 -FETAL	0.8873 (1.0873) 0.8873	125.7 (139.8) 60.4	4.0313 (4.1248) 4.9952	38.819 (38.819) 38.819	3.7793 (3.7793) 3.7793	0.7702 (0.7702) 0.7702	885 (886) 882	1.4 (13.4) 2.8

(h) ^{12}C+^{12}C, E_{Lab} = 1449MeV, Imag. WS(II)Pot.

Table 1: g,h

angle scattering data well. The accompanying imaginary WS potentials are generally weak with values that are similar to the results of past work [12]; and this is indicative of the transparency of the optical potential used for ^{12}C +^{12}C here. In addition, the values of the volume integral of the optical potential per interacting nucleon pair, J_R obtained with the three best-fit folded potentials are very close and much bigger than that of the BDM3Y3-based folded potential (Table 1.0a). Thus, the DDM3Y1-, BDM3Y1- and BDM3Y2-based folded potentials are all seen here to belong to the family of deep refractive potentials, but with these low-energy data, it is difficult to identify which of them is the most appropriate to describe the data.

With respect to elastic scattering data at the energies of 240 MeV and 300 MeV, folding analysis shows a rainbow enhancement of the elastic scattering cross section at large angles in figure 2.0. The difference between the different folded potentials at small distances is reflected in the calculated cross sections at large angles, so it is possible to determine the best folded potential that gives a reasonable description of the data in the whole angular range. A closer look at figure makes it clear that the DDB3Y1 -Fetal and BDB3Y1-Fetal are the most realistic at these angles because they give a better description of the elastic data in the large-angle region than the other two folded potentials. The description of the large-angle data by the BDB3Y2-Fetal and BDB3Y3-Fetal is visibly bad. In order to explain the cause of this degraded performance of the last two potentials, we have plotted the optical potentials used for

the analysis of the elastic data at 300 MeV in the upper region of figure 3.0 in which the weak WS potentials are shown to be close in strength and shape, indicating obviously that the difference in the calculated cross sections at large angles is solely traceable to the difference in the strengths of the folded potentials (underneath the WS potentials in the upper region) at small inter-nuclear distances. Figure 4.0 has been included to show that the BDB3Y3-Fetal is more repulsive that the BDM3Y3-Reid. In the present work, a detailed folding analysis of the ^{12}C +^{12}C data at E_{LAB}= 1016 MeV has revealed that the data are sensitive to the real optical potential down to about 3fm, but no rainbow pattern is observed as shown in figure 5.0. At this incident energy, two categories of the imaginary WS potential: a weak one (WSI) with a depth of about 16 MeV and a strong one (WSII) about 50 MeV deep are used for the analysis. For the 1016 MeV data, the difference in real folded potentials at about 3fm (upper parts of figures 5.0 and 6.0) is seen to influence the calculated cross sections, with the DDB3Y1- and BDB3Y1-Fetal as well DDM3Y1- and BDM3Y1-Reid potentials giving the best fit with the weak WSI potential. Again, the radial shape of the BDB3Y3-Fetal potential is shown in the upper region of figure 5.0 to be much more repulsive at this energy, giving an unreasonable description of the elastic data compared with its attractive BDM3Y3-Reid counterpart in the upper region of Figure 6.0 with a much better performance. With the strong absorptive WSII potential, all the real folded potentials, with the exception of the BDB3Y3-Fetal, have about the same fits to the data (Table l.0f) which are better than those obtained with WSI, but no sensitivity of
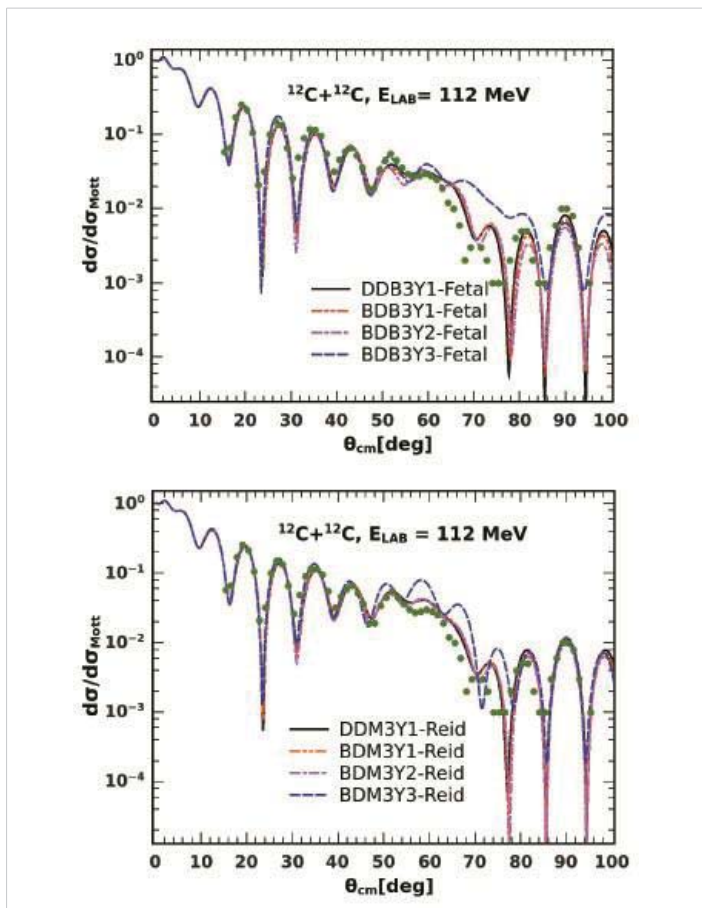
Figure 1: Fits to the ^{12}C +$^{1/2}$C Elastic Data at E$_{Lab}$= 112 MeV by the Four Types of Real Folded Potential Derived from B3Y-Fetal (Upper) and M3Y-Reid (Lower) Alongside the Volume Woods-Saxon [W(R)=WS(I)] Imaginary Potential.
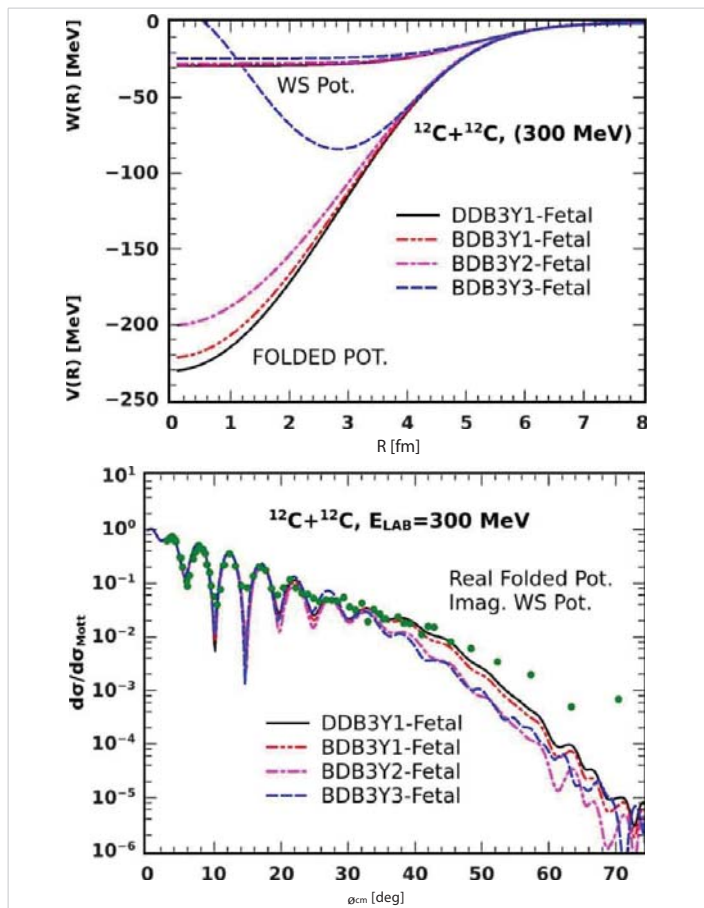

Figure 3: Fits to the ^{12}C +^{12}C Elastic Data at E$_{Lab}$= 300 MeV (Lower Part) Based on B3Y-Fetal with the Radial Shapes of the Real Folded V(R) and Volume Woods-Saxon [WS(I)] Imaginary Potentials (Upper Part).
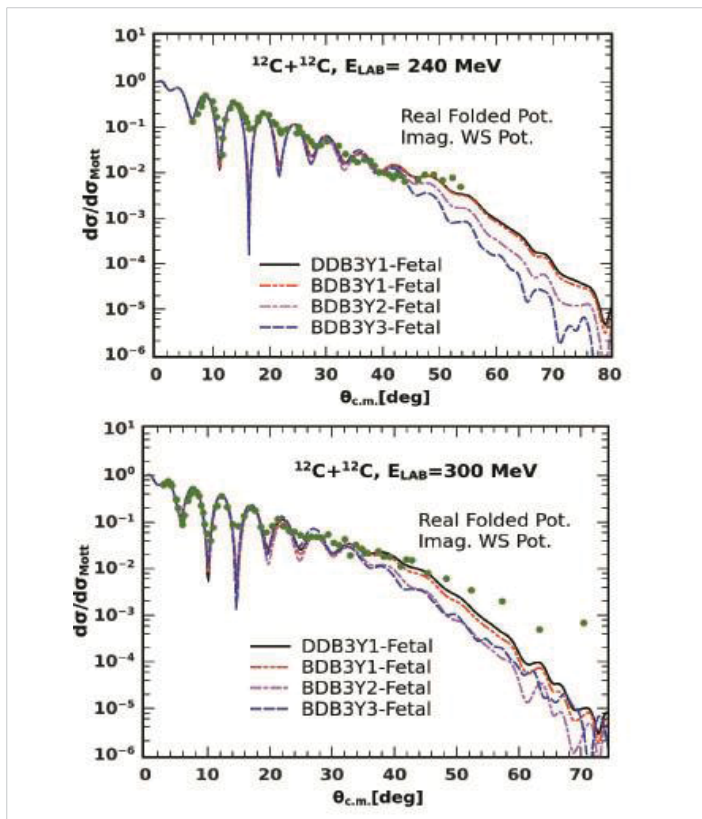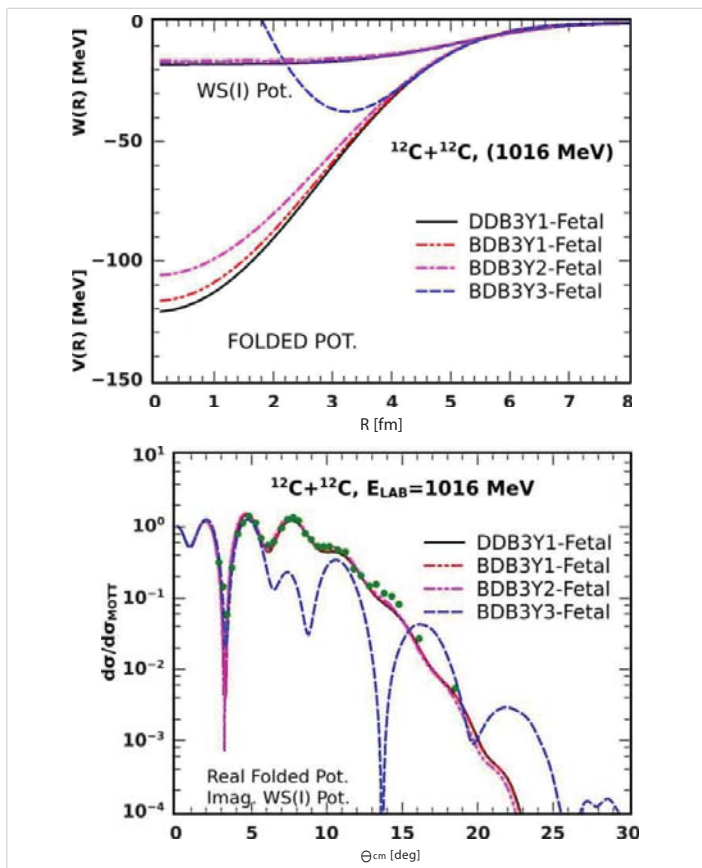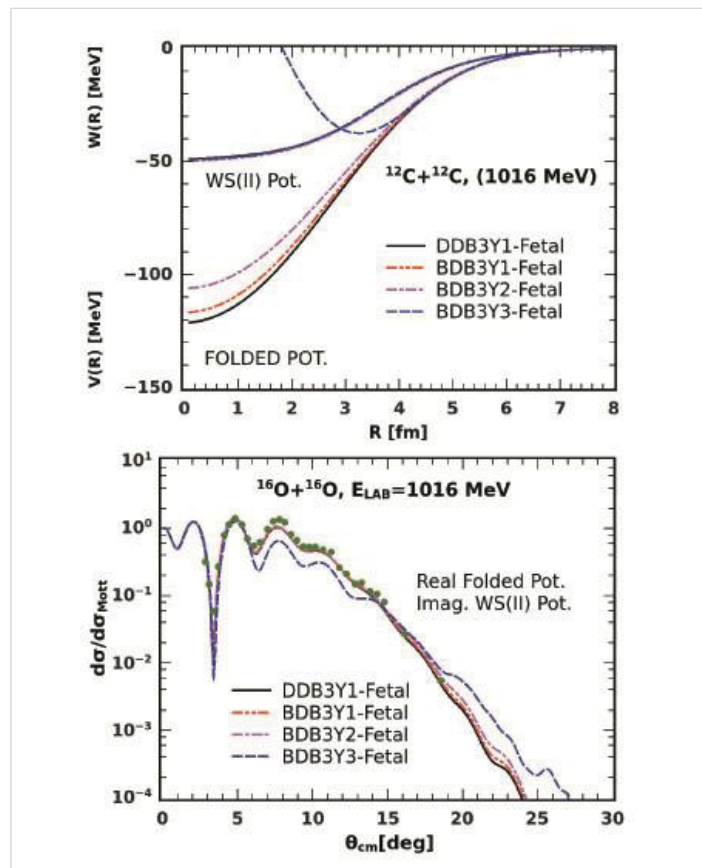

Figure 2: Fits to the ^{12}C+ ^{12}C Elastic Data at E$_{Lab}$ = 300 MeV (Lower Part) and E$_{Lab}$ = 240 MeV (Upper Part) Obtained with B3Y-Fetal.
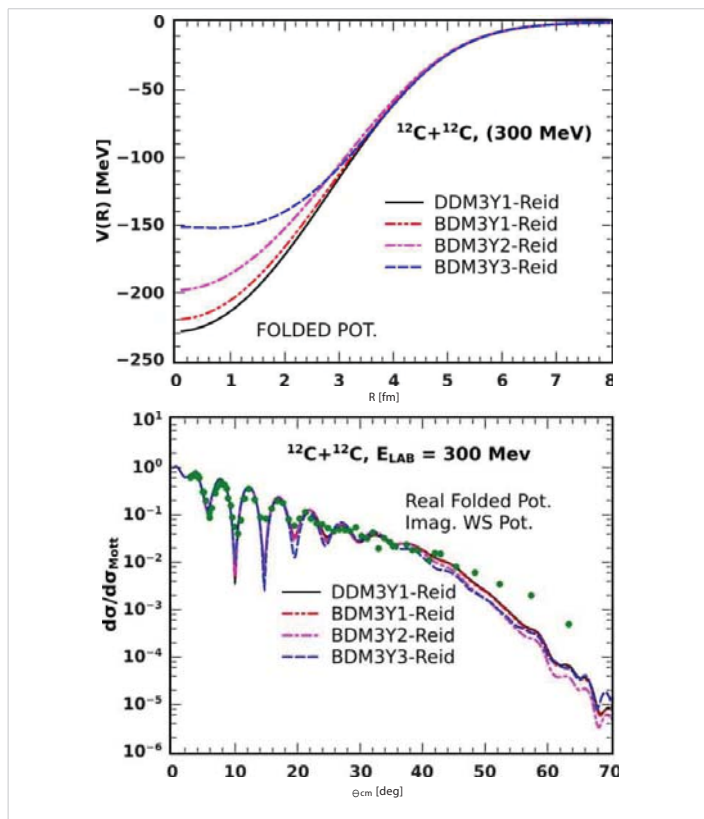
Figure 4: Fits to the ^{12}C+^{12}C Elastic Data at E$_{Lab}$= 300 MeV (Lower Part) Obtained with M3Y-Reid and the Radial Shapes of the Real Folded V(R) Potential (Upper Part).

Figure 5: Fits to the ^{12}C +^{12}C Elastic Data at E_{Lab}= 1016 MeV (Lower Part) Based on B3Y-Fetal with the Radial Shapes of the Real Folded V(R) and Volume Woods-Saxon [WS(I)] Imaginary Potentials (Upper Part).
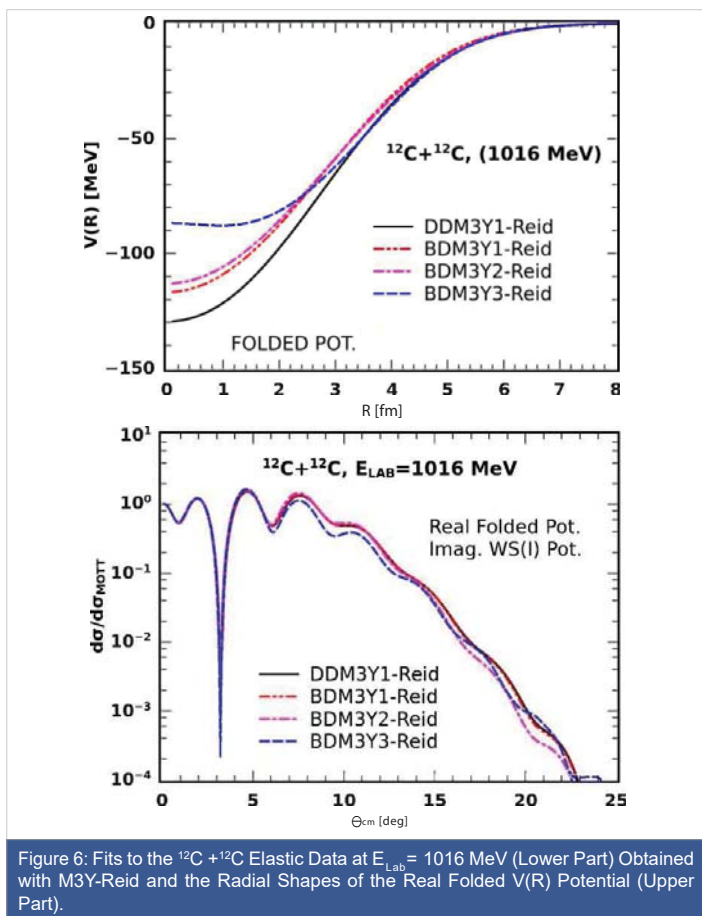

Figure 7: Fits to the ^{12}C +^{12}C Elastic Data at E_{Lab}= 1016 MeV (Lower Part) Based on B3Y-Fetal with the Radial Shapes of the Real Folded V(R) and Volume Woods-Saxon [W(R)=WS(II)] Imaginary Potentials (Upper Part) Used in the OM Analyses.

Figure 6: Fits to the ^{12}C +^{12}C Elastic Data at E_{Lab}= 1016 MeV (Lower Part) Obtained with M3Y-Reid and the Radial Shapes of the Real Folded V(R) Potential (Upper Part).

the data to the real potential at small radii is observed. This is well illustrated in figure 7.0, where the BDB3Y3-Fetal is shown to give a more reasonable description of the elastic data.

On the basis of the information got from the results of our analyses of ^{12}C +^{12}C system so far, it can be reliably said that the DDB3Y1- and BDB3Y1-Fetal folded potentials are the most suitable potentials to fit the data. This conclusion is in agreement with the opinion of previous researchers [12,26] who did extensive work on the same system. Furthermore, it is obvious that the BDB3Y3-Fetal has the poorest description of the ^{12}C +^{12}C data at all energies studied in this work; this is also in perfect agreement with previous work [12,26]. Its performance has been seen to have consistently deteriorated with increasing incident energy. With increasing energy, the direct component of the real folded potential, known to be repulsive [25], has a dominating influence on the exchange component of the real folded potential shown to be attractive in [25], forcing the total real folded potential to be repulsive (Figures 3.0, 5.0 and 7.0) in the small-radius region with attendant performance degradation.

As regards the overall performance of the two effective interactions in the OM analyses of elastic scattering data, the B3Y-Fetal has been shown so far to demonstrate acceptable agreement with the M3Y-Reid. Tables 1.0a - l. Of show that the values of the renormalization factor, N_R obtained with the B3Y-

Fetal are slightly higher than those obtained with the M3Y-Reid so that the corresponding reaction cross sections, a_R for the former are lower than those for the latter in almost all cases. This level of performance by B3Y-Fetal is quite impressive; but the effect of the direct component of its optical potential plays an inhibiting role in the performance of the interaction as the incident energy increases. A well-established trend that both interactions portray is that of the optical potential becoming progressively repulsive as the incident energy increases, which is in agreement with the work of Nuclear Physics scholars [2,11,12,23,30]. However, the optical potential based on the B3Y-Fetal is shown in figures 3.0, 5.0 and 7.0 to grow repulsive with increasing incident energy faster than its M3Y-Reid counterpart in figures 4.0 and 6.0. Of particular note is the rapidity with which the BDB3Y3-Fetal becomes completely repulsive in the small internuclear separation region in figures 3.0 and compared with the corresponding BDM3Y3-Reid in figures 4.0 and 6.0. This effect is shown in the lower part of figure 5.0 to have degraded the description of ^{12}C +^{12}C elastic data by the BDB3Y3-Fetal whose curve does not seem to have any resemblance to the others; but this is not so with the BDM3Y3-Reid optical potential in figure 6.0. Thus, even though it is known that the BDM3Y3-based folded potential, compared with the others, gives the poorest description of the elastic scattering data of nuclear systems [12], available results have proven the folded potential based on the BDB3Y3-Fetal to be poorer than its BDM3Y3-Reid counterpart in the folding analyses of the nuclear system performed in this paper. The folded optical potential based on the BDM3Y2 interaction is seen in both cases in all figures to give worse description of elastic scattering data than the optical potentials derived from the BDM3Y1 and DDM3Y1 interactions. In respect of the last two folded potentials, the agreement between the B3Y-Fetal and M3Y-Reid interactions as seen in all figures from 1.0 to 7.0 is unequivocally impressive, seeing that both effective interactions have shown these optical potentials from the folding analyses carried out in this work to be the best in agreement with the findings of Khoa, et al. [12,26]. The agreement between these best-fit folded potentials, DDB3Y1-Fetal and BDB3Y1-Fetal as well as DDM3Y1-Reid and BDM3Y1-Reid potentials in the optical model analyses in this work is known to imply that the cold nuclear matter has an underlying soft equation of state.

Conclusion

We have carried out the folding analysis of the nuclear reaction invoving ^{12}C +^{12}C nuclei within the framework of the optical model, using a heavy-ion nucleus-nucleus optical potential derived from the B3Y-Fetal effective interaction - a new M3Y-type effective interaction based on variational calculations - in this paper. Accordingly, the differential cross sections associated with the elastic scattering of the nuclear system have been determined at various incident energies with the four folded potentials, DDB3Y1-, BDB3Y1-, BDB3Y2- and BDB3Y3-Fetal. Herein, the results of folding analysis have

reliably shown the DDB3Y1- and BDB3Y1-Fetal to be the best-fit folded potentials, whereas the BDB3Y3-Fetal, followed by the BDB3Y2-Fetal, has the poorest description of the ^{12}C +^{12}C data at all incident energies. This finding puts the B3Y-Fetal in excellent agreement with the previous work of [12] done with the M3Y-Reid whose DDM3Y1- and BDM3Y1- Reid optical potentials have also been found to be the best in this work; and it is known to indicate that the cold nuclear matter is possibly governed by a soft EOS [12,18]. This agreement clearly endorses the B3Y-Fetal-based heavy ion optical potential as an authentic tool for the study of nuclear reactions.

The results obtained in this work have additionally revealed our version of heavy-ion optical potential, based on the B3Y-Fetal, to demonstrate weak absorption in all cases considered, portraying the optical potential to be transparent and making it possible to determine and follow its performance down to very small inter-nuclear distances. This feature is the foundation for testing the B3Y-Fetal and and comparing it with M3Y-Reid effective interaction in this study.

It is hoped that this study will find useful applications in elastic scattering experiments carried out with beams of^{12}C ions in radioactive beam facilities by predicting the best choice of optical potentials to use for the description of nuclear reactions meant to investigate ion-ion interaction. Examples of such facilities are the DC-60 cyclotron at the Institute of Nuclear Physics (INP), National Nuclear Centre (NNC) in Astana, Kazakstan [29,31] and the cyclotron at the Hahn-Meitner Institute (HMI) in Berlin, Germany [24]. Others are the Cooling Storage Ring (CSR) facility HIRFL in China, the Radioactive Ion Beam (RIB) Factory at RIKEN in Japan, the FAIR/GSI in Germany, SPIRAL2/GANIL in France and the facility for Rare Isotope Beams (FRIB) in USA. The findings of this study might also be of good use in Nuclear Astrophysics where nuclear EOS is a major ingredient in calculations; certain nuclear reactions are the main probe of exotic nuclear species; and accurate knowledge of nuclear reaction rates needed for understanding primordial nucleosynthesis and hydrostatic burning in stars requires a combination of new experimental techniques and theoretical efforts.

Acknowledgement

References

1. Carlson VB. Lectures Given at the Workshop on Nuclear Data and Nuclear Reactors: Physics, Design and Safety. Brazil. 2000; 62: 104.

2. Brandan ME, Satchler GR. The Interaction between Light Heavy Ions and What It Tells Us. Physics Reports. 1997; 285: 143-243.

3. Glendenning NK. Direct Nuclear Reactions. World Scientific Publishing Co. Ltd, 5 Toh Tuck Link, Singapore. 2004; 378.

4. Wojciechowski. Quantum Diffraction Grating - A Possible New Description of Nuclear Elastic Scattering. Int J Modern Physics E. 2016; 25: 1-12.

5. Chammon LC, Carlson VB, Gasques LR, Pereira D, De Conti C, et al. Nonlocal Description of the Nuclear Interaction. Bra J Physics. 2003; 33: 1-17.

6. Cook J. Global Optical Model Potentials for Elastic Scattering of 6,7Li Projectiles. Nuclear Physics A. 1982; 388: 153-172.

7. Farid ME, Mahmoud Z MM, Hassan GS. Analysis of Heavy Ions Elastic Scattering Using the Double Folding Cluster Model. Nuclear Physics A. 2001; 691: 671-690.

8. Jackson DF. Nuclear Sizes and Optical Model. Rep Prog Physics. 1974; 37: 55-146.

9. Khoa DT, Oertzen VW, Bohlen HG, Nuoffer F. Study of Diffractive and Refractive Structure in the Elastic 160 +16 O Scattering at Incident Energies Ranging from 124 to 1120 MeV. Nuclear Physics A. 2000; 672: 387-416.

10. Satchler GR. Introduction to Nuclear Reactions 2ed. Macmillan Education Ltd. London. 1990; 317.

11. Satchler GR, Love WG. Folding Model Potentials from Realistic Interactions for Heavy-ion Scattering. Physics Reports (Review Section of Physics Letters). 1979; 55: 183-254.

12. Khoa DT, Oertzen VW, Bohlen HG. Double-Folding Model for Heavy-ion Optical Potential: Revised and Applied to Study 12C and 160 Elastic Scattering. Physical Review C. 1994; 49: 1652-1667.

13. Khoa DT, Oertzen VW, Oglobin. Study of the Equation of State for Asymmetric Nuclear Matter and Interaction Potential between Neutron-Rich Nuclei Using the Density-Dependent M3Y Interaction. Nuclear Physics A. 1996; 602: 98-132.

14. Oertzen VW, Bohlen HG, Subbotin V, Khoa TD. Nuclear Rainbows, Nucleus-Nucleus Potentials and the EOS of Nuclear Matter. International Winter Meeting on Nuclear Physics. Bormio. 2001.

15. Khoa DT, Khan, E, Colo G, Giai NV. Folding Model Analysis of Elastic and Inelastic Proton Scattering on Sulphur Isotopes. Nuclear Physics A. 2002; 706: 61-84.

16. Gontcharn I, Hinde DJ, Dasgupta M, Newton JO. Double Folding Nucleus-Nucleus Potential Applied to Heavy-ion Fusion Reactions. Physical Review C. 2004; 69: 1-14.

17. Ochala I, Fiase JO, Anthony E. Computation of Nuclear Binding Energy and Incompressibility with a New M3Y-Type Effective Interaction. Int Res J Pure Applied Physics. 2017; 5: 5-13.

18. Ochala I, Fiase JO. Symmetric Nuclear Matter Calculations - A Variational Approach. Physical Review C. 2018; 98: 1-8.

19. Ochala I, Gbaorun F, Bamikole JA, Fiase JO. A Microscopic Study of Nuclear Symmetry Energy with an Effective Interaction Derived from Variational Calculations. Int Res J Pure Applied Physics. 2019; 6: 22-33.

20. Ochala I, Fiase JO. A Study of Asymmetric Nuclear Matter with B3Y-Fetal Effective Interaction. A Paper Being Reviewed for Publication in Physical Review C. 2019.

21. Fiase JO, Devan KRS, Hosaka A. Mass Dependence of M3Y-Type Interactions and the Effects of Tensor Correlations. Physical Review C. 2002; 66: 1-9.

22. Bertsch G, Borsowicz J, McManus H, Love WG. Inter- actions for Inelastic Scattering Derived from Realistic Potentials. Nuclear Physics A. 1977; 284: 399-419.

23. Khoa DT, Satchler GR, Oertzen WV. Nuclear Incompressibility and Density Dependent NN Interactions in the Folding Model for Nucleus Potentials. Physical Review C. 1997; 56: 954 - 969.

24. Khoa DT, Oertzen VW, Bohlen HG, Ohkubo S. Nuclear Rainbow Scattering and Nucleus-Nucleus Potential. J Physics: Nuclear Physics. 2006; 34: 1-65.

25. Ochala I. Application of the New M3Y-Type Effective Interaction to Nuclear Matter and Optical Model Analyses. Unpublished PhD Thesis. Benue State University. Makurdi. 2016; 186.

26. Khoa DT, Oertzen VW. Refractive Alpha-Nucleus Scattering; A Probe for the Incompressibility of Cold Nuclear Matter. Physics Letters. 1995; 342: 6-12.

27. Khoa DT, Satchler GR. Generalized Folding Model for Elastic and Inelastic Nucleus-Nucleus Scattering using Realistic Density-Dependent Nucleon-Nucleon Interaction. Nuclear Physics A. 2000; 668: 3-41.

28. Hamada S, Burtebayev N, Gridnev KA, Amangeldi N. Further Investigation of the Elastic Scattering of 160, 14N and 12C on the Nucleus of27A1 at Low Energies. Physica Scripta. 2011; 84: 54-60.

29. Hamada S, Burtebayev N, Amar A, Amangeldi N. Analysis of the Elastic Scattering of 12C on nB at Energy Near Coulomb Barrier Using Different Optical Potential Codes. World Academy of Science, Engineering and Technology. 2010; 69: 54-68.

30. Hodgson PE. The Nucleon Optical Model. World Scientific Publishing Co. Ltd. London. 1994; 421.

31. Hamada S, Burtebayev N, Gridnev KA, Amangeldi N. Further Investigation of the Elastic Scattering of 160, 14N and 12C on the Nucleus of 27A1 at Low Energies. Physica Scripta. 2011; 84: 54-60.